International Journal Of Engineering Research And Development
e- ISSN: 2278-067X, p-ISSN: 2278-800X, www.ijerd.com
Volume 20, Issue 3 (March. 2024), PP. 142-153

Transient Stability Assessment of Nigerian Sub-transmission Network using Artificial Neural Network (ANN)

Itoro Udosen[1], Akaninyene Obot[2], Nseobong Okpura[3], Kufre Udofia[4]
[1,2,3,4]*Department of Electrical and Electronics Engineering, Faculty of Engineering*
University of Uyo, Uyo Akwa Ibom State, NIGERIA
Corresponding Author: Kufre Udofia.

ABSTRACT
With the increasing human population comes increased demand for electricity, making power systems more complex than ever and operating close to their stability limit. Considering the importance of stability in power system security, proposing an approach for enhancing transient stability is essential, considering the consistent uncertainties in power systems. This research proposes an artificial neural network (ANN) to resolve power system transient stability. Cochran's formula determined the number of Monte Carlo samples in the system operations data collected from the case study injection substation. Time domain simulation (TDS) was carried out using DigSILENT Power Factory software, while the ANN training was done using MATLAB toolbox. ANN and TDS were used to compute fault clearing time (FCT) and critical clearing time (CCT) for different fault locations and conditions. A notable finding from the research is that result analysis highlighted that changing the synchronous generator (SG) on a power grid to doubly-fed induction generator converters (DFIG) weakens the system's transient stability. Also, integrating DFIG into the existing network improved the transient stability by decreasing the overall average risk of the system.
Keywords: *Artificial neural network, transient stability, Cochran's formula, Monte Carlo samples, fault clearing time.*

Date of Submission: 10-03-2024 Date of Acceptance: 23-03-2024

I. INTRODUCTION

Power systems are typically highly complicated and entirely nonlinear due to the environment's constant change, which controls the balance between supply and demand for electricity (Olulope et al., 2010). Power system stability is defined as the capacity to quickly recover from disturbances, which, in most circumstances, expose the system to varying degrees of vulnerabilities and lead to unfavourable outcomes that are costly to network operators (Santhoshkumar and Senthilkumar, 2020). According to Lackovic (2017), power system security, also known as resiliency, is assessed based on the possibility that a crucial system infrastructure would continue to provide service to customers despite a disruption. A system that cannot produce enough power cannot be stable, even though two systems with comparable stability margins may differ in security due to instability (Samuel, 2017). Hence, the necessity for power system stability assessment is crucial to the consistent and efficient operation of the power grid. Transient stability assessment must be precisely and accurately assessed using real-time procedures to ensure stable and reliable power supply.

Senyuk et al. (2023) stated that conventional techniques such as numerical integration of a cluster of algebraic differential equations (higher-order differential-algebraic equations) and energy-based evaluation (equal area criterion) were the go-to solutions to power system transient stability problems. Still, they are inefficient and slow to respond to real-time disturbances. Conversely, several modern stability assessment methods have been proposed by several authors, including the use of machine learning, as put forward by Wani et al. (2019), and the use of active learning, as presented by Zhang et al. (2021). Also, Particle Swarm Optimisation (PSO) Technique combined with Deep Belief Network (DBN) was explored as a solution to the stability challenge of power systems by (Liu et al., 2021), as well as the method of Hyperplane presented by (Ma et al., 2023) and that of Convolution Neural Network (CNN) and support vector regressor proposed by (Jin et al. (2023). Among these approaches, Artificial Neural Network (ANN) is the most routine and prevalent due to numerous benefits: modular design and parallel processing capabilities, and it does not require intensive mathematical modelling for training (Gill, 2021). In particular, ANN can quickly map nonlinear relationships between input and output data.

In this study, the major objective is to analyse the Critical Clearing Time (CCT) of the circuit breakers integrated with generators grouped as a single machine linked to an infinite bus system on a segment of the Nigerian power system (Idongesit Nkanga Secretariat injection substation, Uyo). From the conventional point of view, ANN for power studies is generally separated into three major stages: data generation, data preprocessing (features selection/ extraction) and data evaluation. These steps will be adopted in the evaluation of the TSA technique selected for this study. This paper is arranged into sections as follows: Section 1 is the introduction to the study, some related articles are reviewed in Section 2, and the design methodology is presented in Section 3. Results achieved are summarised in Section 4, briefly followed by a conclusion with references appended after that.

II. RESEARCH METHODOLOGY

2.1 Case study site

The selected location for the study is a 33/11 kV injection substation close to Akwa Ibom State Secretariat, Uyo. The substation houses two transformers (T1 and T2) of 15 MVA capacity, each with a direct incoming from a 33 kV line emanating from Afaha-Ube Transmission Station, Uyo. Four outgoings from the station consisting of an 11 kV line supply power to the State Secretariat on the first feeder, IBB way and Federal Secretariat on the second feeder, Udo-Udoma, Shelta Afrique and Oron Road are fed from feeder number three. In contrast, Aka Road is fed from the remaining feeder. The substation also provides an isolation point for the 33 kV transmission line feeding Ibesikpo and Nsit Atai. An earthing transformer with a 300 kVA 33/0.415 kV capacity is installed to improve earth fault protection handling and as an added safety requirement at the substation. A single-line diagram of the station configuration in DIgSILENT Power factory software is shown in Figure 1.

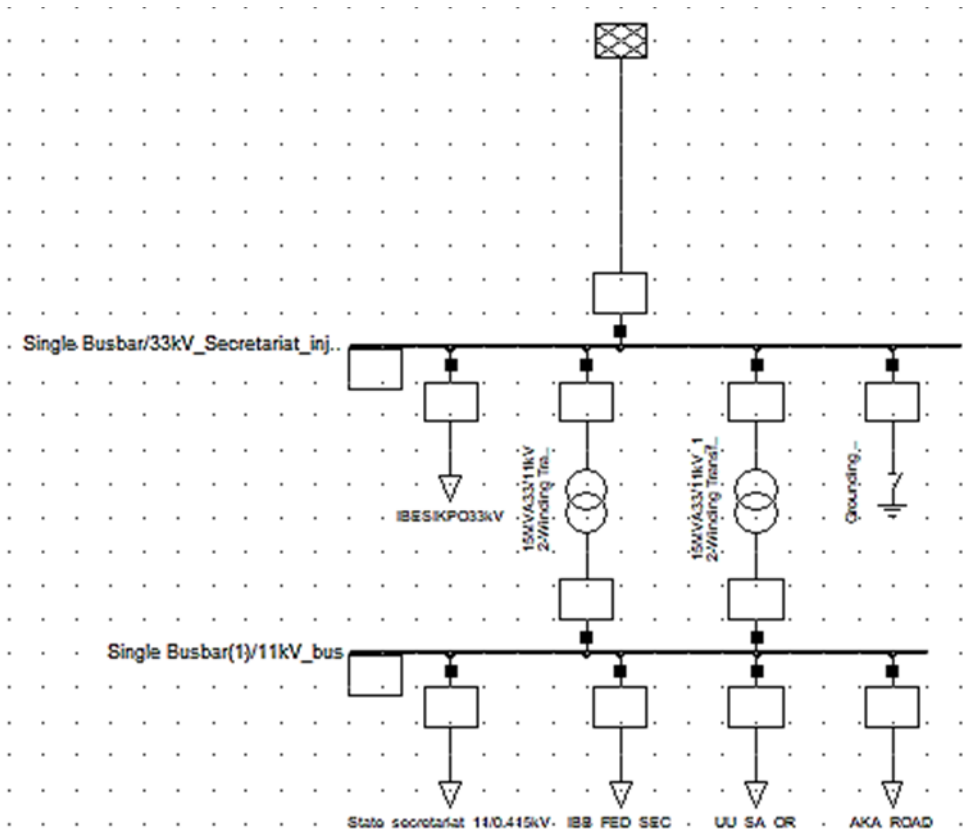

Figure 1: Configuration of Secretariat Injection Substation

The proposed study methodology is shown in Figure 2, where the number for the Monte Carlo (MC) simulation is represented by the symbol i. A static system topology is employed at first, meaning it is presumed that all system components—primarily generators and transformers—will be functioning correctly and fault-free before the occurrence of a fault. The selection of each load value is the following stage. The load bus is chosen using the Gaussian Probability Density Function (PDF). After conducting a load flow analysis to determine the system's state, PDFs are used to select the faulted line, fault type, fault clearing time (FCT), and fault location. For the sake of this study, the fault is produced at time $t = 1\,s$; and a 10-second time-domain stability simulation is run for each sample of MC (system transiently unstable or stable). Based on the highest rotor angle

difference, δmax, these two outcomes are established (the system is stable if $\delta \max > 360$ and unstable otherwise). In other words, the risk of transient instability is evaluated for the i^{th} sample, R_i, if the system is transiently unstable (value is subsequently used for estimation of the average risk index, R_A). The steps to determine N are outlined in Section 3.2.2, after which the MC simulation is terminated at $i = N$ samples, and the value of R_A is computed. The FCT is decremented in phase by about 0.01 s for each MC sample, affecting the non-zero value of R_A, ensuring that R_i and R_A remain zero. The minimal transient stable risk of the system is defined as the value of R_i at $R_A = 0$. As shown in Figure 2, the marginal transient stable risk is the designation for the predicted risk for fault occurrence that is cleared at critical clearing time (CCT).

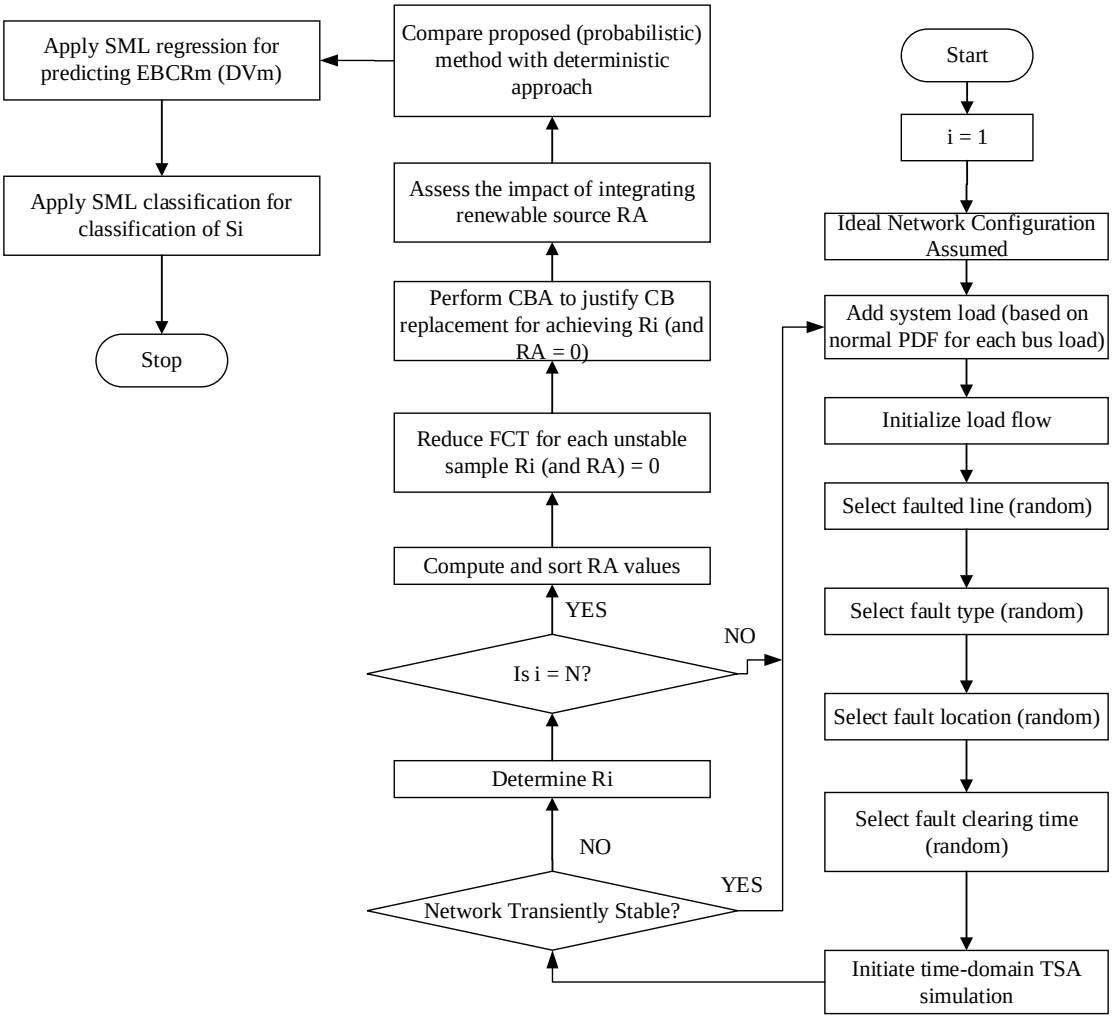

Figure 2: Research methodology

A cost-benefit analysis (CBA) minimises this anticipated risk and justifies changing circuit breakers (CBs) used for nominal fault clearing with the proposed probabilistic model. The next step involves comparing the proposed probabilistic method with a deterministic solution to changing the CB. Lastly, artificial neural network (ANN)-based supervised machine learning (SML) algorithms with provision for classification and regression are utilised in the forecast of the probable value of the benefit-cost ratio (BCR) of n^{th} line (represented by $E{\sim}BCR_n$), and classify transient stability status, S_i, correspondingly. The basic ML outline for the proposed training is also presented in Figure 3.

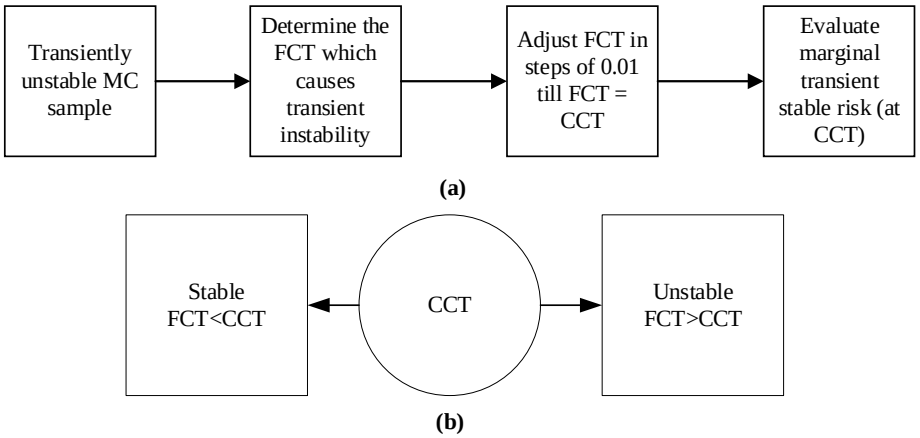

Figure 3: Marginal stability concept

2.2 Modelling of Transient Instability Risk

The severity function in a risk-based approach defines the likelihood and related impact (or effect). Risk is typically defined as the likelihood, probability, and related severity product (McCalley *et al.*, 2004). It is imperative to understand that CCT is the time limit for fault clearing, after which the system becomes unstable. Using the theoretical framework for the risk assessment described in the works by Datta and Vittal (2017), and Li-jie *et al*. (2011), it is assumed that R_i represents the risk of transient instability for the i^{th} MC sample. Additionally, assuming a decision-making interval of half a decade and an average risk index for transient instability of R_A, Equations 1 and 2 mathematically explain the relationship;

$$R_i = P_r(U_i \cap F_i) \times Sev(F_i) = P_r(F_i) \times P_r(U_i|F_i) \times Sev(F_i) \quad (1)$$

$$R_A = \frac{\sum_{i=1}^{N} R_i}{N} = \frac{\sum_{i=1}^{N} P_r(F_i) \times P_r(U_i|F_i) \times Sev(F_i)}{N} \quad (2)$$

where N is the number of MC samples (Each sample shows a faulty line).

Figure 4 gives the flowchart of the ANN technique as applied in the work.
The expression $P_r(U_i \cap F_i)$ represents the joint probability of:

(i) Transient instability event U_i and
(ii) Occurrence of F_i (i^{th} fault event).

In line with conditional probability theory, $P_r(U_i \cap F_i)$ can be written as $P_r(F_i) \times P_r(U_i|F_i)$, as mirrored by Equation 1. $P_r(U_i|F_i)$ is the probability of a transient instability event given F_i has happened, with ranging between denoting values 1 and 0 unstable and stable system (for i^{th} fault event), correspondingly as expressed in Equation 3;

$$P_r(U_i|F_i) = \begin{cases} 1, & \text{for } \delta \max i > 360 \\ 0, & \text{otherwise} \end{cases} \quad (3)$$

$P_r(F_i)$ denotes the probability of F_i (i^{th} fault event) mathematically defined in Equation 4;

$$P_r(F_i) = P_r(F_{oi}) \times P_r(F_{Li}) \times P_r(F_{Ti}) \quad (4)$$

where $P_r(F_{Ti})$, $P_r(F_{Li})$ and $P_r(F_{oi})$, represent the fault type, fault location and the probability of fault event, respectively, for the i^{th} MC sample (Abapour and Haghifam, 2012; Papadopoulos and Milanovic, 2017). Taking to an arbitrary F_{oi} be variable preceding an even probability mass function (PMF) on the interval $\{1, 2, 3, \dots, N_L\}$ as defined in Equation 5.

$$P_r(F_{oi}) = \begin{cases} \frac{1}{NL}, & 1 \le i \le NL \\ 0, & \text{otherwise} \end{cases} \quad (5)$$

where NL is the total number of power lines in the pilot system. Also, taking F_{Li} to be an arbitrary variable preceding a continuous uniform PDF evaluated within 0 to 100, as expressed in Equation 6.

$$P_r(F_{Li}) = \begin{cases} \frac{1}{Np}, & 1 \le i \le Np \\ 0, & \text{otherwise} \end{cases} \quad (6)$$

where $Np = 100$.

$P_r(F_{Ti})$ is selected based on PMF values given in Table 3.1, where $x = 1, 2, 3$ and 4 symbolise three-phase fault (LLL), double line-to-ground (LLG), line-to-line (LL) and single-line-to-ground (LG) fault, respectively (Abapour and Haghifam, 2012). $Sev(F_i)$ measures the gravity of F_i for transient instability mathematically given in Equation 7.

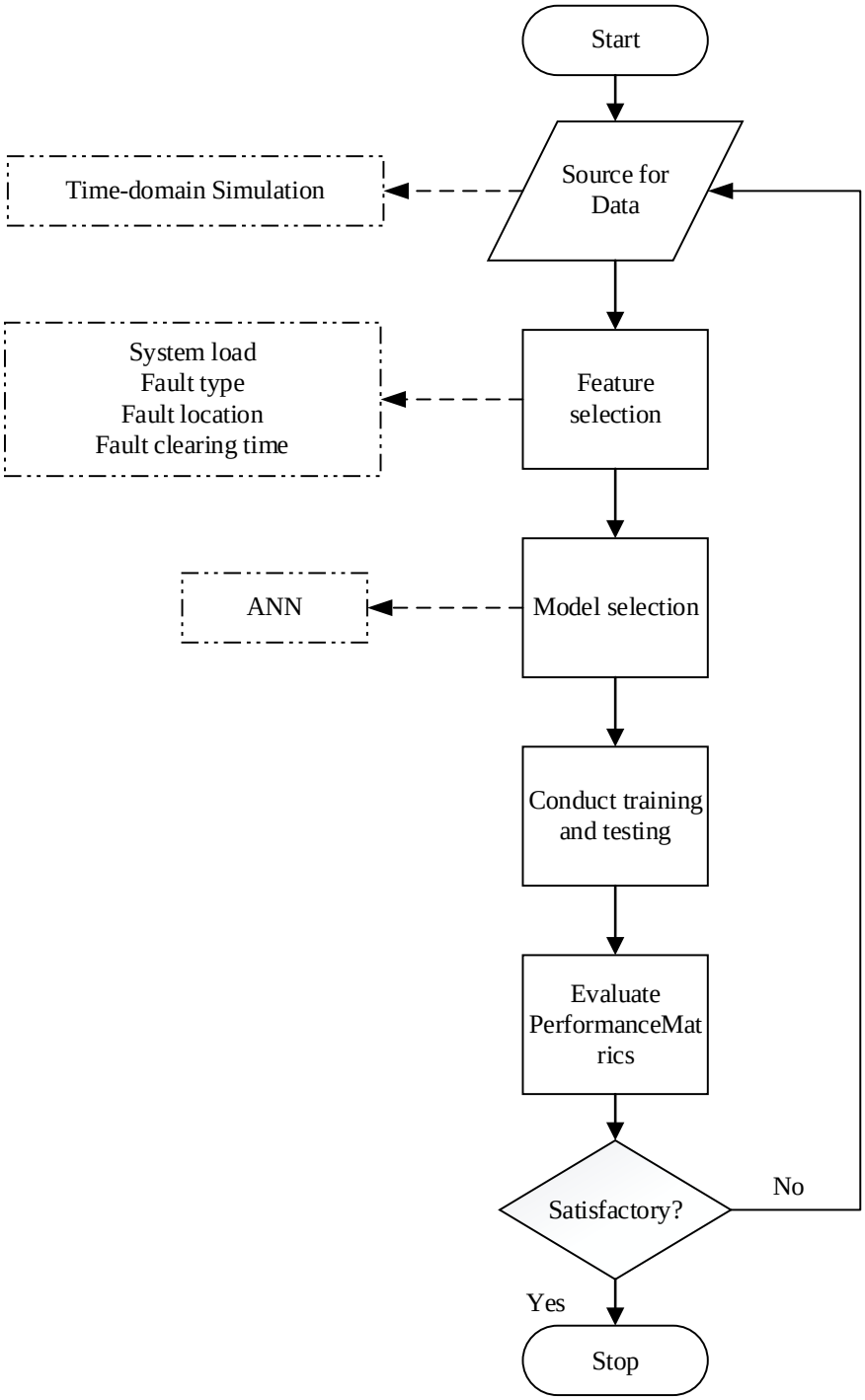

Figure 4: Basic framework of applied ANN technique

$$Sev(F_i) = \begin{cases} |TSI_i|, & \text{if } TSI_i < 0 \\ 0, & \text{otherwise} \end{cases}, 0 < TSI_i < 1 \quad (7)$$

where TSI_i is the transient stability index for the i^{th} MC sample as presented in Equation 8.

Table 1: Probability fault types

x	$P_r(F_{Ti})$
1	0.7
2	0.17
3	0.1
4	0.05

Source: Shahzad (2021)

$$TSI_i = \frac{360-\delta \max i}{360+\delta \max i} \quad (8)$$

where, $\delta \max i$ represents the post-fault maximum rotor angle difference between any two synchronous machines in the system at the time of a fault on the i^{th} line, commonly expressed in degrees (Abapour and Haghifam, 2012). When the TSI_i is negative, it means that the system is momentarily unstable for the i^{th} MC sample. Using a normal PDF with a mean equal to the predicted values and an accompanying standard deviation is appropriate to recreate the uncertainty in each load prediction (Billinton, 1979). Taking the PDF for load at i^{th} bus as $f(X_i)$ as presented in Equation 9;

$$f(X_i) = \frac{1}{\sqrt{2\pi\sigma i^2}} e^{\frac{-(X_i-\mu i)^2}{2\sigma i^2}} \quad (9)$$

whereμi and σi are the mean and standard deviation (10% of the mean) of the predicted peak load for i^{th} bus.
A normal PDF with a mean and standard deviation of 0.9 s and 0.1 s is assumed to come before the FCT (Miao *et al*., 2013; Faried *et al*., 2010; Shi *et al*., 2014). Using Equation 10's mathematical representation of the i^{th} MC sample's transient stability status S_i, the two modes (stable and unstable) are easily related.

$$S_i = \begin{cases} 1, & \text{if } TSI_i < 0 \text{ (unstable)} \\ 0, & \text{if } TSI_i > 0 \text{ (stable)} \end{cases} \quad (10)$$

Hence, for a transiently stable system at i^{th} MC sample, the value of S_i will be 0 and 1 otherwise. Equation 10 contains the data adopted to train the ML model for the classification challenge.

2.3 Cost Benefit Assessment (CBA) Modelling

The cost-benefit analysis (CBA) is a valuation procedure used to determine the viability of a power project and develop an economic case for investment. The premise of the investment decision is on benefit-cost ratio - BCR (BCR greater than 1 justifies the investment while BCR less than 1 does not. This study uses CBA to ascertain whether the current CBs (TSA technique) are due for replacement with more efficient ones for decreasing transient stability enhancement. R_i (as well as R_A) to zero.

2.4 Costs Implication of Transient Instability Risk

Evaluating the indirect and direct expenses incurred owing to synchronous generators (SGs) tripping due to two components—replacement cost and CB replacement cost—allows one to quantify the cost impact of transient instability (Abapour *et al*., 2016).

a. Cost of Replacement: The generating energy at an original cost of C_{ORIG} (N/MW) must be substituted for h hours by a superior cost-intensive generation, with a cost of C_{EMER} (N/MW) as the emergency generation, especially for the generation lost for n^{th} SG, P_{Gn}. Taking $C_{rep}{}^{n}$ as the replacement cost of n^{th} SG, as given in Equation 11.

$$C_{REP}n = (C_{EMERG} - C_{ORIG}) \times P_{Gn} \times h \quad (11)$$

It is assumed that C_{ORIG} is N16000/MW and C_{EMERG} is N32000/MW. The lost time h is presumed to be 10 units. Hence, the replacement cost (for i^{th} unstable MC sample), for n transiently unstable SGs, is given in Equation 12.

$$C_{REPi^n} = 200 \times \sum_{n=1}^{j} P_{Gn} \quad (12)$$

b. Cost of Repair and Start-Up: Given that the SG must be repaired and restarted, CRS^i taken to be the cost for transient instability for i^{th} transiently unstable sample. Mathematically,

$$C_{RS^i} = 60{,}000 \times n_i \quad (13)$$

where; n_i is the number of synchronous machines that are transiently unstable for the i^{th} MC sample. Hence, the cost related to an i^{th} transiently unstable sample, C_i, is

$$C_i = C_{REPi^n} + CRS^i.$$
$$= \left(200 \times \sum_{n=1}^{j} P_{Gn}\right) + (60{,}000 \times n_i) \quad (14)$$

Thus, the cost accompanying the risk R_i [$R_i = P_r(F_i) \times Sev(F_i)$] given by C_i. This expression then becomes the financial gains made by lowering R_i to zero (marginal stability risk).

2.5 Number of Samples Used

The required number of MC samples (N) used for the time-domain simulation was determined using Cochran's formula (see Equation3.15) with a 2% margin of error and 95% confidence level illustrated as presented by Equation 3.15 as follows:

$$n_0 = \frac{p(1-p)z^2}{e^2} \quad (15)$$

where n_0 is Cochran's sample size recommendation, e is the margin of error, z is the reliability level, and p is the population proportion.

For confidence level of 95%, z = 1.96, Equation 15 becomes;

$$n_0 = \frac{0.5 \text{ x } (1-0.5)\text{x}1.96^2}{0.02^2} = 2401$$

For small population, a modified Cochran formula to determine new sample size is used as shown by Equation 16 as thus;

$$n = \frac{n_0}{1+\frac{(n_0-1)}{N'}} \quad (16)$$

From system operation data collected, a threshold population size ($N^{'}$) of 631 is used to determine the sample size as presented in Equation 17,

$$n = \frac{2401}{1+\frac{(2401-1)}{631}} \cong 500 \quad (17)$$

Note that the value of $N^{'}$ used in the calculation is based on the estimated number of fault incidences (major and minor faults) recorded in a year.

III. RESULTS AND DISCUSSION

3.1 Time Domain Simulation (TDS) Results

The test system in Figure 1 is modelled and simulated using the DIgSILENT software to aid in interpreting the system operation data from the Secretariat Injection Substation effectively. The external grid (Afaha-Ube) was modelled as a generator of 6th order with an automatic voltage regulator. The same environment was used to compute the critical fault clearing time (CCT), vital in establishing the model performance. The CCT value of the investigated network was first calculated using a time domain simulation and a trial-and-error methodology. This was done to produce sufficient data for the ANN model training. The sampled data is produced by applying a single contingency (three-phase fault) to line 1 on the test system at various fault locations while maintaining constant generated power. Each sampled piece of data is assessed based on the behaviour of the generator rotor angle. For the analysis, eight fault locations with percentage representations were considered. At 30, 40, 50, 60, 70, 80, 90, and 100% from bus 2, there were superimposed defects (11 kV). The reactive power of the generator utilised in the model, which is kept constant, is 80 MVAR, and the true power of the generator is 100 MW. Each fault incidence was initialised, and then it was cleaned by isolating the faulted line. On line 1, the fault was introduced at 0.1 seconds; at 0.15 seconds, the line was removed, erasing the fault. Table 2 displays the recorded value for CCT for the TDS at several fault locations.

Table 2: Critical clearing time (CCT) and fault location

Fault	Fault location from 11 kV bus (%)	Fault location from 11 kV bus (km)	CCT_{TDS} (Sec)
F_1	30	26.04	0.53
F_2	40	34.72	0.54
F_3	50	43.40	0.59
F_4	60	52.08	0.60
F_5	70	60.76	0.61
F_6	80	69.44	0.63
F_7	90	78.12	0.66
F_8	100	86.80	0.71

Preparatory to TDS, the state variable was initialised using power flow. With an integration time step of 0.01 seconds, the simulation was conducted for 20 seconds. The critical time threshold (CCT) was determined by moving the FCT to the point at which an increase in time will cause the system to become unstable. Data were gathered for each fault location, and 100 samples were taken 0.1 seconds after the fault was fixed. The features of the generator speed, rotor angle, active power, reactive power, and terminal voltage have been chosen and are considered significant for determining CCT. Eight sites were taken into account, resulting in a size of 800 data points for five features (100×8). The total amount of data has dimensions of 800×5.

Three fault cases were also tested by introducing third order generator Doubly Fed Induction Generator (DFIG) at bus 1 (case 1), bus 2 (case 2), and the two buses (bus 1 and 2 simultaneously) to replace

the SG as highlighted in the research model from Figure 3.2. This is to model the system's reaction to including renewable energy (wind energy) furnished with terminal voltage control to the studied electricity grid. The increased generation from the simulated results increased the capacity of the studied grid by an average of 43%. The typical PDF, with a mean of 20 MW and a standard deviation of 2 MW, is used to depict the active power forecast error distribution of each DFIG. The active power from the expanded capacity is likewise represented as 20 MW and 2 MW, respectively. For the three cases, R_A values obtained from the DIgSILENT Power Factory were 0.0052, 0.0061, and 0.0074 for the different cases.

3.2 Artificial Neural Network Training Outcome

Regression: On the MATLAB toolbox interface, a multi-layer feed-forward neural network (NN), generally called multi-layer perceptron (MLP) NN, was utilised. Levenberg-Marquardt algorithm was used for the data training because of its characteristic fast convergence and better performance, along with ten (10) hidden layers (selected on a trial-and-error approach) between the input and output. The logistic activation function (the tan-sigmoid activation function) was used to evaluate the hidden layer neurons, and the identity activation function was used for the neuron output layer. The weights and biases were iteratively adjusted until minimum square error (MSE) was obtained between the target value and network output. The substation operation data collected was divided into training (70%), testing (15%) and validation (15%) subsets. This was done with the aid of MATLAB toolbox. The performance of the transient stability assessment using the trained ANN was done by calculating the minimum square error (MSE) between the estimated CCT ($\mathrm{CCT_{ANN}}$) and the target CCT ($\mathrm{CCT_{TDS}}$).

The first step in applying ANN model to TSA is to use collected operations data under different fault conditions to train the ANN algorithm. From the computed number of samples in the previous subsection, each fault condition is iterated using 500 random MC samples. Each sample randomly chooses fault location, system load, fault type, and FCT (based on the defined characteristics). Two regression and classification approaches were applied with the aid of ANN to improve the computation efficiency, especially concerning FCT. For regression, input and output data were selected from the operation data for the case study site for the ANN training model. The output of the regression training is presented in Figure 5, while the algorithm learning performance curve is given in Figure 6. Epoch 166 of the trained algorithm has the best validation performance. A crucial hyperparameter for the ML algorithm is this number (epoch). The epoch determines how many full transitions of the entire training dataset go through the algorithm's learning phase. At every epoch cycle, the internal algorithm parameters of the dataset are updated. The mean squared error (MSE) value at epoch 160 is 0.0030722. The ANN training took a time of 1 second with 166 epochs on an Intel Core i5 10^{th} generation processor with 16 GB RAM configuration. The training ended after 166 epochs since the approach of the early stoppage was used to improve the accuracy of the trained network.

Classification: A similar procedure with the recorded classification error was applied for the classification task. The choice of input and output data for the ANN classification model was the first stage. System transient stability status (S_i), a chosen output was obtained from the ANN using network system load, fault kind, fault location, and FCT as inputs.

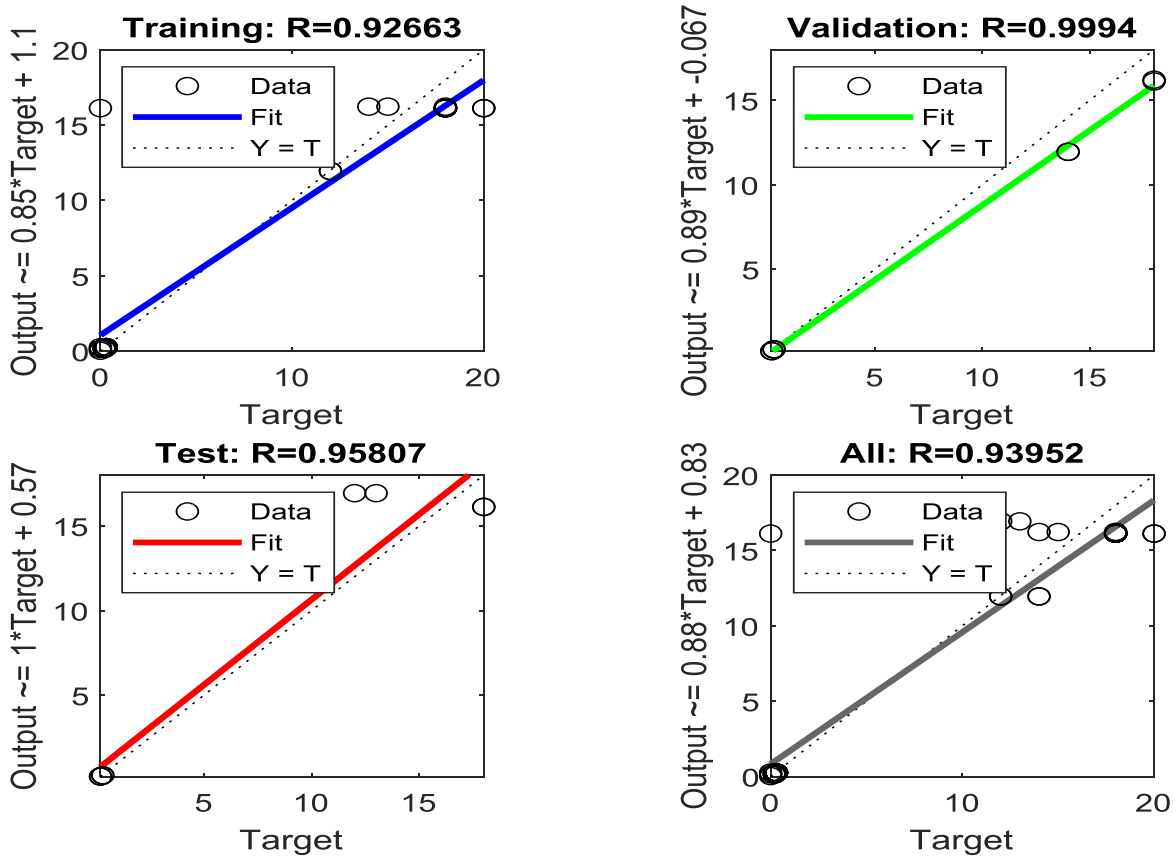

Figure 5: Performance of regression using the correlation coefficient (R) plot

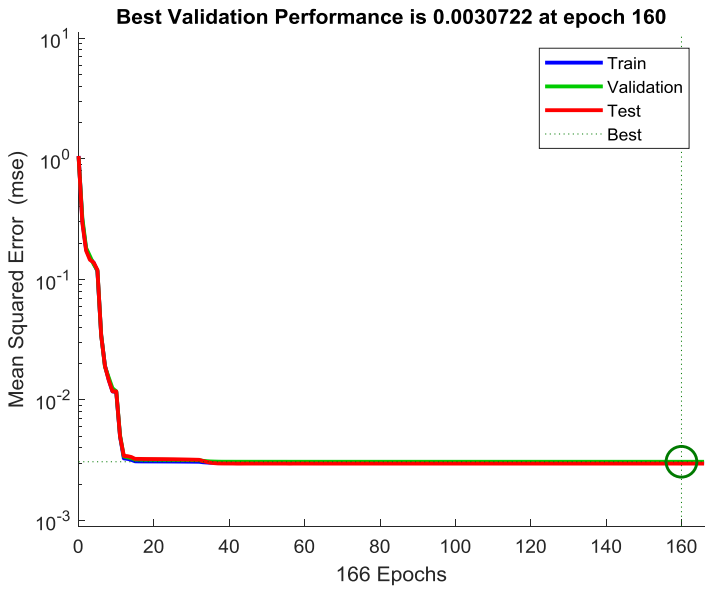

Figure 6: Learning curve of trained data

A total of 9180 training data samples were used (510 for each line). The randomised data division was set at 6426 (70 percent), 1 377 (15%), and 1 377 (15%), correspondingly, for training, validation, and testing. A similar algorithm to the one used for the regression (Levenberg–Marquardt back propagation algorithm) was also adopted for the ANN classification training. Confusion matrix was applied to assess the performance of the trained classifier, as presented in Figure 7.The observations along the diagonal (the green boxes) indicate correctly classified samples, while the opposite diagonal indicates incorrect predictions.

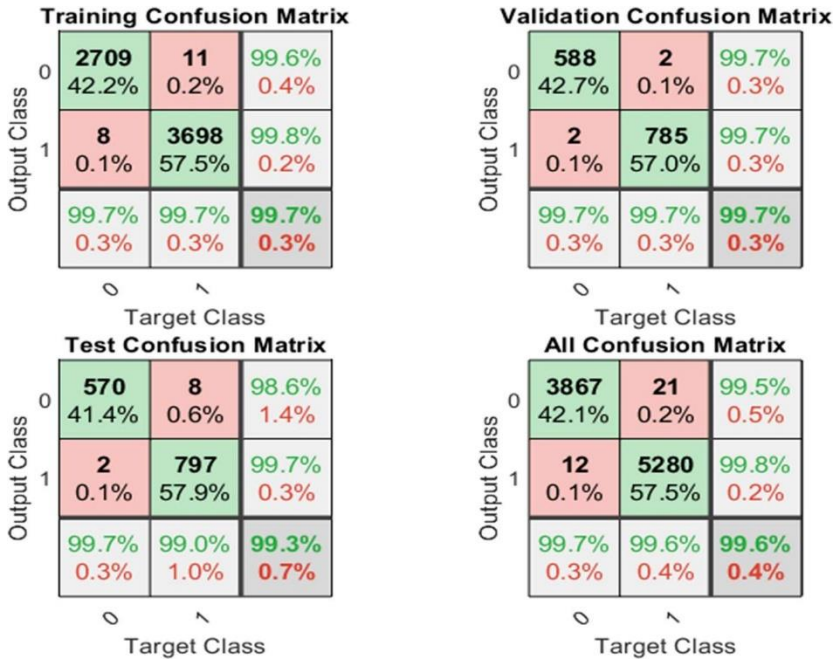

Figure 7: Transient stability performance confusion matrix

A receiver operating characteristics (ROC) plot for an ML classification model with accurate discrimination passes through the upper left corner (100 %sensitivity, 100 %specificity), meaning that its area under the curve (AUC) is equal to 1. The classification accuracy increases as the AUC approaches 1. The classification accuracy (CA) for the confusion matrix (whole sample) is quite good (99%), as can be shown in Figure 8. This infers that for any input (fault location, faulted line, system load, fault type, and FCT), the ANN model correctly predicted the Si status 99 out of 100 times. Similarly, it has been found that the error rate is typically 1%. Additionally, Figure 8 shows the error histogram acquired for the ANN classifier. The values of the various performance metrics obtained for classification and regression are listed in Table 3, where it is clear enough that the values for all of the performance measures fall into the high accuracy range (> 0.98). Therefore, it can be concluded that the trained ML algorithm correctly (99%) categorised the transient stability state, Si, and predicted DV_m.

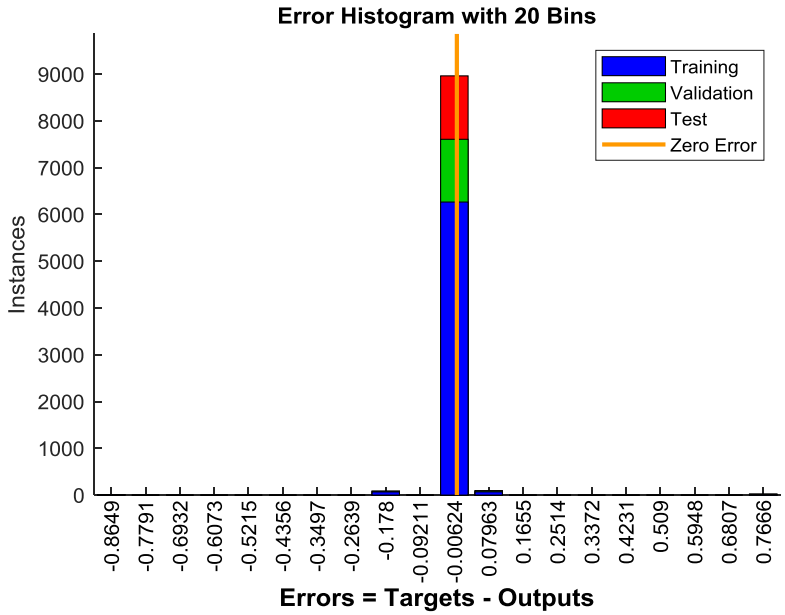

Figure 8: Histogram of classification error

Table 3: Summarised performance metrics

	Metric	Training	Validation	Testing	All
Regression	R	0.927	0.999	0.958	0.940
Classification	CA	0.997	0.997	0.993	0.996
	AUC	0.997	0.994	0.995	0.999

3.3 Performance Assessment

In this study, TSA was carried out using TDS and ANN. To initialise TDS, the required MC samples were determined with the aid of Cochran's formula with 2% margin of error and 95% confidence level. The number of MC samples used for iteration was determined to be 2401. An abridged two-bus network consisting of 33 kV (bus 1) and 11 kV (bus 2) was modelled in DIgSILENT Power Factory. The incoming from Afaha-Ube was modelled as a 6^{th} order generator, while the feeders were the simulated load. The impact of renewable energy inclusion on the studied grid stability was investigated, and it was observed that the order of the generator model determined the overall system stability.

On the other hand, results achieved from the ANN algorithm showed a trend of elongated FCT and CCT with increased fault location. Hence, prolonged system instability modelled and quantified in terms of time. The analysis proved that changing SG to DFIG weakens the transient stability. Furthermore, by lowering the system's average risk, adding DFIG to an existing network increased transient stability. Regression and classification SML techniques based on ANNs were utilised to improve the computation efficiency. These algorithms' performance measurement measures showed that they could be used to achieve the desired result of cutting down on calculation times.

Pandey *et al.* (2007) focused on bulk power systems with no transient stability assessment as this study did. Also, no evaluation was done on his proposed work by including renewable energy sources. Shahzad (2021) and Shahzad (2022) utilised the IEEE 14-bus network to model their algorithms with no real network operation data to test their findings, as was obtainable in this study.

IV. CONCLUSION

This study has focused on power system transient stability analysis on a substation close to the Akwa Ibom State Secretariat. Findings based on station-specific operation data highlighted the different response characteristics of the system based on dynamic fault events and disturbances resulting from the integration of renewable energy into the grid. Two automated analyses - TDS and ML (ANN) - were applied to the system to appropriately improve the overall system response to disturbances and performance concerning CCT. From TDS results, increased distance resulted in increased CCT, with prolonged network instability being the consequence. The values of different performance metrics for classification and regression presented in this report show an apparent inclination towards a high accuracy range (> 0.98) for all metrics considered. Consequently, inference can be drawn that the trained ML algorithm predicted DV_{m} and classified transient stability status, S_{i} with a high accuracy of approximately 99%.

REFERENCES

[1]. Abapour, M., and M. Haghifam. 2012. Probabilistic Transient Stability Assessment for on-line Applications. *Electrical Power and Energy Systems* 42:1, 627–634.

[2]. Billinton, R. 1979. Probabilistic Evaluation of Transient Stability in a Multimachine Power System. Proc. of the Inst. of Elect 126:4), 321–326.

[3]. Datta, S., and V. Vittal. 2017. Operational Risk Metric for Dynamic Security Assessment of Renewable Generation. IEEE Transactions on Power Systems 32:2, March. 1389–1399.

[4]. Faried, S. O., R. Billinton, and S. Aboreshaid. 2010.Probabilistic Evaluation of Transient Stability of a Power System Incorporating Wind Farms. IET Renewable Power Generation 4:4, July. 299–307.

[5]. Gill, N. S. 2021. Artificial Neural Networks Applications and Algorithms. *XenonStack, April 2021*, 1–24. https://www.xenonstack.com/blog/artificial-neural-network-applications

[6]. Jin, W., Zhou, B., Althubiti, S. A., Alsenani, T. R., and Ghoneim, M. E. 2023. Transient stability assessment of power systems using support vector regressor and convolution neural network. *Sustainable Computing: Informatics and Systems*, *37*, 100826. https://doi.org/10.1016/J.SUSCOM.2022.100826

[7]. Lackovic, V. 2017. *Power System Transient Stability Study Fundamentals* (Issue 877).

[8]. Li-jie, C., L. Jing, and C. Jing. 2011. Research of risk-based Security Assessment of Power System, in Proc. DRPT, Weihai, China, pp. 1335–1340.

[9]. Liu, W., Hao, D., Zhang, S., and Zhang, Y. 2021. Power System Transient Stability Assessment Based on PSO-DBN. *2021 6th International Conference on Power and Renewable Energy, ICPRE 2021*, 333–337. https://doi.org/10.1109/ICPRE52634.2021.9635219

[10]. Ma, R., Zhan, M., Jiang, K., Liu, D., Hu, et al. 2023. Transient Stability Assessment of Renewable Dominated Power Systems by the Method of Hyperplanes. *IEEE Transactions on Power Delivery*. https://doi.org/10.1109/TPWRD.2023.3281814.

[11]. McCalley, J., Asgarpoor, S., Bertling, L., Billinion, R., Chao, et al. 2004. Probabilistic Security Assessment for Power System Operations. In Proc. IEEE Power Energy Soc. Gen. Meet, Denver, USA., pp. 1–9.

[12]. Miao, L., J. Fang, J. Wen, and W. Luo. 2013. Transient Stability Risk Assessment of Power Systems Incorporating Wind Farms." Journal of Modern Power Systems and Clean Energy 1:2, 134–141.

[13]. Olulope, P. K., Folly, K. A. A., Chowdhury, S. P., Chowdhury, S. P., and S. P. Chowdhury. 2010. Transient stability Assessment using Artificial Neural Network Considering Fault Location. *Iraq Journal of Electrical and Electronic Engineering*, *6*:1, 633–637. https://doi.org/10.1109/icit.2000.854241.

[14]. Papadopoulos, P. N., and J. V. Milanović. 2017. Probabilistic Framework for Transient Stability Assessment of Power Systems with High Penetration of Renewable Generation. IEEE Transactions on Power Systems 32:4, 3078–3088.

[15]. Samuel, I. A. 2017. *A New Voltage Stability Index for Predicting Voltage Collapse in Electrical Power System Networks*.

[16]. Santhoshkumar, T., and Senthilkumar, V. 2020. Transient and small signal stability improvement in microgrid using AWOALO with virtual synchronous generator control scheme. *ISA Transactions*, *104*(xxxx), 233–244. https://doi.org/10.1016/j.isatra.2020.05.006

[17]. Senyuk, M., Safaraliev, M., Kamalov, F., and Sulieman, H. 2023. Power System Transient Stability Assessment Based on Machine Learning Algorithms and Grid Topology. *Mathematics 2023, 11, 525*, *11*:3, 525. https://doi.org/10.3390/MATH11030525

[18]. Shahzad, U. (2021). Application of supervised machine learning for prediction of probabilistic transient stability. *Australian Journal of Electrical and Electronics Engineering*, *19*:1, 65–78. https://doi.org/10.1080/1448837X.2021.2013418

[19]. Shahzad, U. 2022. A risk-based machine learning approach for probabilistic transient stability enhancement incorporating wind generation. *Australian Journal of Electrical and Electronics Engineering*, *20*:2, 106–121. https://doi.org/10.1080/1448837X.2022.2112293.

[20]. Shi, L., S. Sun, L. Yao, Y. Ni, and M. Bazargan. 2014. Effects of Wind Generation Intermittency and Volatility on Power System Transient Stability. IET Renew. Power Gener 8 (5, July), 509–521.

[21]. Wani, M. A., Bhat, F. A., Afzal, S., and Khan, A. I. 2019. *Advances in Deep Learning*. *57*(January). https://doi.org/10.1007/978-981-13-6794-6